Geophysical demonstration of the absence of correlation between lineaments and hydrogeologically usefull fractures: case study of the Sanon hard rock aquifer (central northern Burkina Faso)

Donissongou Dimitri Soro, Mahamadou Koïta, Chabi Angelbert Biaou, Eli Outoumbe, Jean-Michel Vouillamoz, Hamma Yacouba, Roger Guérin

Geophysical demonstration of the absence of correlation between lineaments and hydrogeologically usefull fractures: case study of the Sanon hard rock aquifer (central northern Burkina Faso)

Donissongou Dimitri SORO[a,b*], Mahamadou KOITA[a], Chabi Angelbert BIAOU[a], Eli OUTOUMBE[a], Jean-Michel VOUILLAMOZ[c], Hamma YACOUBA[a], Roger GUERIN[b]

[a] Laboratoire hydrologie et ressources en eau, Institut International d'Ingénierie de l'Eau et de l'Environnement, 01 BP 594 Ouagadougou, Burkina Faso

[b] Sorbonne Universités, UPMC Univ Paris 06, UMR 7619, METIS, case 105, 4 place Jussieu, 75252 Paris Cedex 05, France

[c] Université Grenoble Alpes, IRD, CNRS, Grenoble INP, IGE, CS 40700, 38058 Grenoble Cedex 9, France

Email authors:

dimitri.soro@gmail.com, mahamadou.koita@2ie-edu.org, angelbert.biaou@2ie-edu.org, outoumbe@gmail.com, jean-michel.vouillamoz@ird.fr, hamma.yacouba@2ie-edu.org, roger.guerin@upmc.fr

*Corresponding author

Abstract

The conceptualization of hard rock aquifers in terms of their geometry and structure has undergone considerable progress over the last two decades. Despite these advances, hydrogeologists are still divided by the models used to describe two central concepts: (i) the influence of weathering processes on hydraulic conductivity; (ii) the influence of tectonics on the hydraulic conductivity of hard rock aquifers. In order to provide further insight into this debate, the present study proposes a conceptual model for hard rock aquifers, based on an integrated hydrogeological and geophysical approach, using information acquired at different scales. The data and observations used for this case study were derived from the Sanon experimental site, located in Burkina Faso, which is presently exposed to a Sudano-Sahelian climate.

The methodological approach consisted firstly in developing a description of the site's weathering profile at the scale of a borehole, based on lithologs and electrical resistivity logs. In a second step, the site's ridge to ridge (longitudinal) weathering profile was established from several 2D resistivity sections crossing a maximum number of lineament structures, which in some prior studies were considered to be the superficial manifestation of tectonic fractures.

The results show that at that scale the weathering profile is comprised of three main layers, which from top to bottom are referred to as: the saprolite, the fissured layer and the fresh rock. This weathering profile model is consistent with other models proposed in recent years, suggesting that the hydraulic conductivity of hard rock aquifers is a consequence of weathering processes, rather than tectonic fracturing. Tectonic fractures are not visible on the 2D sections of the ridge to ridge profiles, and the lineaments originally thought to be overground representations of tectonic fractures are likely to have different origins. The lack of a substantial correlation between tectonic lineaments and fractures appears to account for the high incidence of negative boreholes in hard rock aquifers, where the siting of drillings has systematically been based on lineament studies and on geophysical studies looking for vertical fractures such as profiling and vertical electrical sounding. There is thus a need to revise current hydrogeological concepts and methodologies to site wells based on tectonic fractures represented by lineaments.

Keywords: Hard rock aquifer, weathering profile, lineaments, tectonic fractures, electrical resistivity, West Africa.

1. Introduction

More than 80% of West Africa subsoil is composed of hard rocks (MacDonald and Davies, 2000) that are not intrinsically porous and pervious. However, they were or are still subjected to weathering processes which gave them hydrodynamic properties, in particular fracture permeability (Lachassagne *et al.*, 2011). Thus, weathered zones of these hard rocks constitute aquifers which are increasingly exploited for the population water supply (e.g. Dewandel *et al.*, 2010, 2008; Carter and Parker, 2009; Taylor *et al.*, 2009; Chilton and Foster, 1995). These aquifers are sustainable water resources for West African rural populations (Courtois *et al.*, 2009). Indeed, the groundwater stored in hard rock aquifers is geographically well distributed (Lachassagne and Wyns, 2005) and offers an alternative to pollution-prone surface water resources. Access to this groundwater is generally through boreholes. Thousands of boreholes have been drilled since the 1980s in the context of rural water supply projects. As many as 25% to 60% (e.g. Vouillamoz *et al.*, 2014; Courtois *et al.*, 2009; Lutz *et al.*, 2007) of the boreholes are “dry”, indicating the complexity of hard rock aquifers and the need to develop suitable conceptual models and suitable methodologies to site boreholes.

Over the past twenty years, many advances have been made in the development of representative conceptual models for these aquifers. As an example, the role of fractures as hydraulic barriers was highlighted by Lachassagne *et al.* (2011). Some studies conclude that the fracture hydraulic conductivity of hard rock aquifers is due to weathering processes (e.g. Su *et al.*, 2015; Koïta *et al.*, 2013; Lachassagne *et al.*, 2011; Courtois *et al.*, 2009; Dewandel *et al.*, 2006; Maréchal *et al.*, 2004; Wyns *et al.*, 2004), while others consider fracture hydraulic conductivity to be of tectonic origin (e.g. Kouamé *et al.*, 2010; Kamagaté *et al.*, 2008; Razack and Lasm, 2006; Wright and Burgess, 1992).

For the former group, the hydraulic conductivity of hard rocks is inherited from weathering profiles, within a fissured stratiform layer located immediately below the unconsolidated saprolite. In this model, the weathering profile includes, from top to bottom: (i) laterite, iron or bauxitic crust, which can be absent due to erosion or rehydratation of hematite in a latosol; and (ii) saprolite, a clay-rich material derived from prolonged *in situ* decomposition of the fresh rock, which has a thickness of a few tens of meters. The saprolite layer can be further divided into two sub-units (Wyns *et al.*, 1999): the alloterite sub-unit (consisting of mostly clays), and the isalterite sub-unit (in which weathering processes preserve the original rock structure) whose effective porosity is normally between 3% and 10%. The weathering profile also includes: (iii) a fissured layer, which is generally characterized by dense fissuring in the first few meters below its top, with a relative high hydraulic conductivity and rather a low porosity; and finally (iv) fresh rock, which is unfractured hard rock and has a very low hydraulic conductivity and storativity (Maréchal *et al.*, 2004). This model of a horizontally stratified reservoir has been successfully applied to various hard rock aquifers in India (Dewandel *et al.*, 2006, 2010), Ivory Coast (Koïta *et al.*, 2013), South Africa and East Africa (Taylor and Howard, 2000).

In the latter case, the hard rocks are considered to be highly heterogeneous, with their hydraulic properties deriving mainly from tectonic origins and lithostatic decompression. During drilling campaigns, the project supervisors in charge of selecting borehole sites have always searched for soil surface lineaments. These are supposedly the surface representation of subvertical fractures, and are detected by suitable processing of satellite images and aerial photographs.

This paradigm has oriented (1D) electrical resistivity sounding campaigns and borehole drilling (Savadogo *et al.*, 1997; Wright and Burgess, 1992), but fails to explain the current 30% to 40% of dry boreholes (Brunner *et al.*, 2006; Sander, 2006). In view of this situation, the question arises as to whether some of these concepts, which the majority of applied hydrogeologists still consider to be relevant, should be reviewed. The aim of the present study is, thus, to provide answers to this question, by using an integrated approach to characterize and propose a conceptual model of a hard rock aquifer, based on information obtained at different scales.

Our methodology, firstly, involved a description of the weathering profile at borehole scale (1D) through the use of lithologs and electrical resistivity logs. Next, the weathering profile was characterized from ridge to ridge on a watershed by electrical resistivity sections (2D), crossing the maximum number of lineaments identified in previous studies.

The study was carried out at the Sanon experimental catchment site, which had already been the subject of groundwater research in the 90s (Compaoré, 1997; Compaoré *et al.*, 1997; BRGM-Aquater, 1991).

In the following section we describe the methods used for the borehole scale investigations and to determine the ridge to ridge weathering profile. A conceptual model of the weathering profile is then proposed. Finally, our model is compared with the two aforementioned concepts (i.e. hydraulic properties due to weathering, and due to tectonic fracturing revealed by lineaments).

2. Description of the Sanon experimental site

2.1. Location and climate

The Sanon experimental site is located within a hydrological entity (surface sub-catchment of Red Volta river), approximately 40 km northwest of Ouagadougou (the capital city of Burkina Faso) between the longitudes of 1°45'35" and 1°42'42"W, and the latitudes of 12°25'55" and 12°29'10"N. It has a surface area of 14 km^2 and is characterized by a very weakly contrasted relief (Fig. 1). The ridges in this area are mainly covered by iron crust, between 350 and 370 m amsl. They form the boundaries of the surface hydrological entity. The central part of the site is characterized by a relatively broad, flat-bottomed valley, sloping from east to west.

The climate in this area is of the Sudano-Sahelian type, with a short rainy season (from June to September) and a long dry season (from October to May). The mean annual rainfall varies between 700 and 900 mm and the temperature ranges between 25 and 40°C.

2.2. From regional to local geology

The geology of Burkina Faso is characterized by rocks belonging to the West African craton, which has one of the lowest seismicities in the world, characterized by earthquakes with a magnitude less than 4. This craton comprises two distinct entities: the Reguibat Shield in the North, and the Leo Shield, also referred to as the Man Shield, in the South (Fig. 2). These two groups are separated by sedimentary formations called the Taoudeni basin. In the Leo Shield, Paleoproterozoic formations crop out in nine West African countries: Burkina Faso, Ivory Coast, Ghana, Guinea, Liberia, Mali, Niger, Senegal and Togo (Lompo, 2010). The age of the formations is not exactly known, and diverse estimates have been proposed in different studies (e.g. Kouamelan *et al.*, 2015; Lompo, 2010; Feybesse *et al.*, 2006; Egal et al., 2002; Guiraud, 1988). However, this shield can be subdivided into two domains:

- The Archean or Kenema-Man domain (Fig. 2). This is characterized by two orogenic cycles: the Leonian, dated from 3500 to 2900 Ma, and the Liberian, dated from 2900 to 2600 Ma.
- The Baoule-Mossi domain (Fig. 2) is dominated by the Paleoproterozoic era. It was recorded in the second domain of the Eburnean orogenic cycle dated from 2400 to 1600 Ma. According to various studies (Sattran and Wenmenga, 2002; Savadogo *et al.*, 1997), the Eburnean orogenic cycle is characterized by: (i) the fracturing of an ancient hard rock, in two directions (N15° to N20°E and N100° to N120°), (ii) the intrusion of granodioritic dykes, and (iii) roughly adjusted isoclinal series and very tight folds. Furthermore, it is noteworthy that the formation of granites and migmatites began around 2100 Ma, during a period when already

metamorphosed materials from the Antebirimian age were affected by migmatization responsible of “gray” granites and migmatites. Between 2000 and 1800 Ma, the general Birimian metamorphism occurred, followed by the formation of leucocratic granites. This granitization led to the silicopotassic recrystallization of “gray” granites and migmatites. As for the green rocks, which are complex structures composed of metabasites, these were formed at the end of the Birimian and are characterized by a metamorphosed and folded series that is unconformable with neighboring formations.

The study area is located on the Central Plateau of Burkina Faso, and is composed of rocks that are representative of the West African hard rocks. They were emplaced during the Eburnean orogeny.

The local geology of the study site is characterized by a patchwork of migmatite, gneiss and granite, and green rocks, with a sandy, arenitic or lateritic weathering cover. As there are no bedrock outcrops, it is difficult to accurately map the areas occupied by these formations.

3. Material and methods

The methodological approach applied during this study consisted firstly in analyzing lithologs, to determine the type and thickness of the various layers of the weathering profile and also of course the lithology of the parent rock. Electrical resistivity values were then assigned to each layer of the weathering profile. These were derived from electrical resistivity logs recorded in boreholes and new observation wells, from which cuttings were used to set the lithologs. Finally, a 2D Electrical Resistivity Tomography (ERT) section was determined from ridge to ridge, and classified in geological terms on the basis of the corresponding “resistivity range – layers of the weathering profile”, derived from electrical logs. These investigations were performed at two different scales: those carried out at borehole scale, and those carried out at catchment scale (from ridge to ridge).

3. 1 Description of the weathering profile at borehole scale

The vertical structure of the weathering profile was mainly based firstly on the interpretation of 18 lithologs, and secondly on the interpretation of electrical logs recorded in 12 unequipped boreholes and observation wells.

The lithologs were either recorded at boreholes and observation wells drilled during the present study, or derived from previous observations (BRGM-Aquater, 1991). The interpretation of these lithologs was enhanced through the use of additional drilling data (drilling speed and change of drilling tools), and the observation of artificial outcrops as traditional brickworks (pits used for the manufacture of laterite bricks) on the hillsides covered by a lateritic iron crust. The cuttings were studied in order to assess the nature and geometry of the different components of the weathering profiles, corresponding to the various geological formations within the catchment.

Pole-pole electrical resistivity logs (Chapellier, 1987) were then recorded and interpreted, in order to affect resistivity values to the various layers of the weathering profile. The pole-pole array used an inter-electrode spacing (AM) of 80 cm. The electrical resistivity logs were recorded in 10 boreholes extending through the entire thickness of the weathering profile, and in two observation wells extending through the saprolite only. In each borehole, the measurements were made where the well is screened and below the piezometric level, as such measurements are only possible there.

3. 2 Description of the ridge to ridge weathering profile

Most of the ridge to ridge weathering profile measurements were made using ERT, leading to the elaboration of a 2D model of sub-surface resistivity, which is supposed to vary vertically and horizontally along the profile (Dahlin, 2001). This technique involves the implementation of two distinct processes, described as the following:

• Field investigations

Field measurements were carried out with a Syscal R1-Plus Switch 72 resistivimeter (Iris Instruments). Wenner-alpha and Wenner-beta arrays (Dahlin and Zhou, 2004) were used, with an inter-electrode spacing of 5 m. The combined use of these two arrays allows the vertical and horizontal resolutions of the measurements to be optimized, while providing a good depth of investigation (Descloitres *et al.*, 2008b; Massuel *et al.*, 2006). Three profiles: PS1, PS15 and PSaG from northern ridge to southern ridge and passing through by the boreholes S1, S15 and SaG respectively were achieved. They were linked to the ridges from North to South (Fig. 1). Their lengths are as follows: 2875 m for PS1, 2400 m for PS15 and 1800 m for PSaG (Fig. 1). The profile directions were set to: N15° (PS1) and N08° (PS15 and PSaG) due to the presence of obstacles (houses, sacred sites) in the field, thus traversing the highest possible number of lineaments, as proposed by previous studies (Kabré, 2012; BRGM-Aquater, 1991). This approach was designed to validate these lineaments, which are supposed to be the surface representation of bedrock fractures. The advantage of making measurements close to existing boreholes is that their lithologs can be used as a reference for the calibration of geophysical data.

• Data processing: inversion, calibration and classification

The raw field measurements were initially filtered to remove any corrupt data points: measurements having a different magnitude, or a difference in apparent resistivity greater than one third of the neighboring values were deleted. This prevented the occurrence of various artifacts. Following this pretreatment, the data were inverted, calibrated and classified.

The aim of the apparent resistivity inversion process was to reconstruct the “true” sub-surface resistivity distribution (Olayinka and Yaramanci, 2000). The first step in this process involved the elaboration of an initial model, which was iteratively improved by comparing the observed and computed responses, with respect to the model parameters (Olayinka and Yaramanci, 2000). The DC2DInvRes software (Günther, 2004) was used for this data processing step. For the inversion, the L1-norm (blocky or robust) constraint was used to provide well-contrasted resistivity units.

The inversion quality was assessed in terms of the Root Mean Squared (RMS) and Chi-square (Chi^2), using Eqs. (1) and (2).

$$RMS = \sqrt{\sum_{i=1}^{n}((x_{data,i} - x_{model,i})/x_{data,i})^2/N} \quad (1)$$

$$Chi^2 = \sum_{i=1}^{n}((x_{data,i} - x_{model,i})/\varepsilon)/N \quad (2)$$

where N represents the total number of measurements

The RMS measures the difference between the interpreted apparent resistivity values given by the model (x_{model}) and the measured values (x_{data}). Chi^2 corresponds to the difference between the terms x_{model} and x_{data}, normalized by the error, noted ε, corresponding to each measurement (estimated error, depending on the array used, the inter-electrode spacing, the injected voltage and the measured values of apparent resistivity). In order to develop a mathematical model that accurately reproduces the measured values of apparent resistivity, the RMS (defined above) must be as small as possible, and the noise on the electrical measurements must be minimized. In addition, extreme values can affect the computed value of RMS. Chi^2 can thus be a better estimator of the model's accuracy, since it provides a representative estimation of the errors due to resistivity measurements (Günther, 2004). However, as it has been shown that low values of RMS or Chi^2 do not guarantee that the model provides an accurate representation of the subsurface (Descloitres *et al.*, 2008a), it is nevertheless important to refer to lithologs for geophysical data calibration.

The geophysical models obtained by inversion were clustered (e.g. Chaudhuri *et al.*, 2013), according to the resistivity ranges corresponding to the “saprolite”, “fissured” and “fresh rock” layers obtained from the electrical resistivity logs.

4. Results

4.1. Weathering profile across the borehole

It is not possible to propose a geological map of the area allowing to locate migmatites, gneisses, granites and green rocks because there is a low density of boreholes and no outcrops of parent rock. Consequently, it is difficult to map the areas occupied by the various geological formations. However, a brief description of the lithology of the parent rock is presented below, and the geological formations identified from each lithology is mentioned on figure 1.

- Description of the lithologs

The analysis of 18 lithologs revealed that the weathering profiles of all formations (granite, migmatite and green rocks) observed in the catchment have a classical vertical structure. This includes, from top to bottom, the following components: (i) a saprolite which can be divided into two sub-layers: alloterite (rich in kaolinite and where the structure of the parent rock is no more visible) and isalterite (with abundant quantities of clay and sand and where the structure of the parent rock is still visible). The mean thickness of the saprolite layer is 37.6 ± 7 m and it varies between 22 and 49 m; (ii) a fissured layer, in which water strikes were observed during drilling with a down-the-hole hammer (this is characterized by cuttings containing elements of weathered rock as well as fresh bedrock). The mean thickness of fissured layer is 13.8 ± 8 m and it varies between 2.5 and 35 m. The high value of the standard deviation (relative to the mean) may indicate a large difficulty in estimating the thickness of this layer, as the only way to characterize it is the location of permeable fractures; and (iii) a fresh rock which is unfractured. In addition, the profiles are usually covered by a thin layer of sand and laterite, except on their ridges where, in some places, they are covered by an about 8 m thick iron crust (Fig. 3).

Although the structure of the weathering profile described above is standard, significant differences in thickness have been observed within the same geological formations. These differences were also observed as a function of the topography, or the relative position of the profile with respect to the lowest central part of the catchment.

On the migmatites, the weathering profile is thicker at the lowest central part of the catchment, where the saprolite (alloterite and isalterite) reaches an average thickness of 49 m (litholog from borehole S1). In some cases we noted the disappearance of the isalterite layer, in favor of the alloterite layer. The profile thickness decreases gradually with distance from the center of the valley (axis through the lowest central part of the catchment), and reaches its smaller values, an average of 22 m (litholog from borehole S14), at the ridges.

No marked differences in weathering profile thickness were observed on the green rocks and granites, since very few lithologs were available for these geological formations (3 for the green rocks and 3 for the granites). However, thin saprolite layers are observed on the green rock formations of the interfluves.

- Description of the iron crust profile

The analysis of iron crust profiles at a traditional brickwork site (Fig. 3) revealed a ferruginous slab at the top. This has a conglomerate appearance at the surface, highlighted by glazed purple nodules. The latter are merged into the mass of the slab. Where they are broken, these nodules reveal fine pores. An indurated clay-sand matrix is located below the ferruginous slab, and has a horizontal laminated structure, under which a second indurated clay-sand matrix appears at an average depth of 4 m. The latter is uncracked and has many non-interconnected voids. The structure of the iron crust described here is likely to influence the surface flows, and in catchment areas where the alteration profile is covered by an iron crust, this structure can be expected to have an impact on the infiltration process. It surely promotes the surface flows and reduces infiltration.

- Interpretation of electrical resistivity logs

The variations in electrical resistivity as a function of depth, derived from electrical resistivity logs (Fig. 4), allowed electrical resistivity ranges to be allocated to each layer of the weathering profile as defined by the lithologs (Fig. 5). With this profile, it is found that the electrical resistivity varies as a function of depth and inside the same layer (Fig. 4), thus revealing his heterogeneity. In this figure, it can also be seen that the transition from one layer to another is characterised by a progressive variation in resistivity, suggesting that there is no abrupt change in facies along the weathering profile. This is particularly highlighted between the fissured layer and the fresh rock. Indeed, in the fissured layer, there is a dense fissuring in the first few meters and a downward-decreasing density of fissures. This makes difficult the identification of the boundary between these two layers. All these observations do not allow the geometric boundary between successive layers of the weathering profile to be determined with certainty.

Statistical analysis of the full set of data derived from the electrical resistivity log reveals that the median values of electrical resistivity for the “saprolite”, “fissured” and “fresh rock” layers are respectively 120, 418 and 1291 Ω.m.

The representation of the lower and upper quartiles of resistivity for each layer of the weatehring allows to well differentiate between the three main layers of the medium. Lower quartiles 228 Ω.m and 871 Ω.m characterize the base of the “fissured layer” and the “fresh rock”, respectively. These two values were then used to define boundaries between the three layers: for the “saprolite”, “fissured” and “fresh rock” layers, the following electric resisitivities ranges were thus selected: [0; 228 Ω.m[, [228; 871 Ω.m[and [871; 100 000 Ω.m[. A resistivity threshold of 60 Ω.m was also used to distinguish the most conductive portions of the saprolite (Chapellier, 1987). The resulting resisitivity ranges make it possible to propose a geological interpretation for the 2D resistivities measured in the catchment, as described in the following section.

4.2. Description of the ridge to ridge 2D weathering profile

4.2.1. Geophysical interpretation

- 2D electrical resistivity cross-section

Two-dimensional cross-sections of the 2875 m apparent resistivity profile PS1, passing through borehole S1, are shown in Figs. 6a and 6b. The resistivities were pretreated by removing outlier values (small blank areas in these pseudo-sections). This figure reveals the presence of low apparent resistivities (blue) at the center, and high apparent resistivities further from the center (brown) of both sections.

The interpreted resistivity model, resulting from the joint inversion of both series of apparent resistivities (Wenner-alpha array and Wenner-beta array) (Fig. 6c), indicates the presence of a highly conductive zone (resistivities less than 60 Ω.m) at the center of the model. This zone corresponds to the central valley of the catchment, and can be seen to become thinner at increasing distances from the center. Highly resistive (greater than 871 Ω.m) superficial environments can also be distinguished at the two upper ends of the model. These coincide with the northern and southern rigdes, covered by a hardened iron crust.

4.2.2. Geological interpretation

Analysis of the geological models (Fig. 8), derived from our classification of the 2D resistivity sections (Fig. 7) PS1, PS15 and PSaG, shows that:

i) for each profile, the geometry of the geological model (1D) with respect to the positions of boreholes S1, S15 and SaG is consistent with the geometry of the lithologs recorded at these boreholes.

ii) the presence of four layers corresponds to the classical conceptual model for hard rocks, namely alloterite and isalterite layers (which together form the “saprolite layer”), a fissured layer and a fresh rock. The resistive cover (resistivity greater than 871 Ω.m) is due to the presence of an iron crust on the ridges, whereas in the valley it corresponds to lateritic dry sand.

iii) the saprolite layer is sensibly thicker in the central valley (37-48 m) as compared to the ridges area (10-30 m), and is characterized by a high clay content (resistivity less than 60 Ω.m). In this part of the catchment, the fissured layer is thinner (5-10 m) as compared to the other areas (4-20 m). The fresh rock (resistivity greater than 871 Ω.m) is situated at a depth of approximately 50 m in the valley. The profile thickness decreases at the ridges, where the alloterite layer is almost nonexistent. At the ridges, the weathering profile is characterized by thickening of the fissured layer and a fresh rock high, which is more pronounced at the southern ridge.

The geological model described above provides a good explanation for the behavior of the Sanon hydrogeological catchment. Indeed, the presence of an iron crust on the ridges facilitates the runoff of rainwater towards the central valley, which becomes the preferred groundwater recharge zone as a consequence of its sandy surface structure. Runoff water accumulates within the valley and infiltrates below the surface, leading to localized recharging of the aquifer. This in turn provides a credible explanation for the existence of a piezometric dome area, confirmed by the piezometric map (Compaoré *et al.*, 1997).

4.2.3. Validation of the lineament structures

In the different geophysical and geological ridge to ridge models (Figs. 7 and 8), there is no visible evidence of tectonic fractures. The lineaments identified on the lineament map (Fig. 2) can thus not be considered as the representation of surface tectonic fractures.

5. Discussion

The weathering profile model developed in the present study is consistent with other recently proposed models (e.g. Langman *et al.*, 2015; Koïta *et al.*, 2013; Lachassagne *et al.*, 2011; Courtois *et al.*, 2009; Dewandel *et al.*, 2006; Wyns *et al.*, 2004). These models assume the hydraulic conductivity of hard rocks to be inherited from weathering profiles, rather than from tectonic fractures. Indeed, the ERT did not reveal the discontinuities identified in previous studies through the use of aerial photography and Landsat 7 satellite imagery. In geological models based on the classification of electrical resistivity values, there is no visible trace of tectonic fractures; and it is unlikely for lineaments to be recognized as confirmed surface representations of tectonic fractures. This lack of correlation between lineaments and tectonic fractures could explain the high rate of negative wells drilled in hard rocks, despite the use of lineament analyses during many drilling campaigns. Although several authors have described or characterized the assumed structure of hard rock aquifers and stated that their fracturing is of tectonic origin (e.g. Kamagaté *et al.*, 2008; Razack and Lasm, 2006; Savadogo *et al.*, 1997; Wright and Burgess, 1992; Faillat and Blavoux, 1989), this hypothesis has not been demonstrated (Lachassagne *et al*., 2011). The latter authors assert that tectonic fracturing cannot be invoked as a genetic concept to explain the origin of secondary fissures/fractures in hard rocks. According to the same authors, in tectonically stable areas such as most of the world's hard rocks regions, the tectonic fracturing theory requires:

i) a tectonic process to create the fracture. The occurrence of such fractures is in fact very rare in both time and space;

ii) that the resulting fracture be permeable. A tectonic fracture is generally a complex structure, which is far from being systematically permeable;

iii) that the resulting tectonic fractures reach the subsurface (i.e. the depth of the hard rocks water well). In practice, tectonic fractures do not extend up to the regions closest to the surface;

iv) that permeable fractures remain unsealed for long periods of time (on a geological time-scale), whereas rejuvenation is in practice counteracted by sealing: tectonic fractures tend to be old and are sealed accordingly.

These arguments infer that tectonic fractures are located in the sub-surface, at a depth of several kilometers where they cannot be reached by standard well-drilling techniques, which have a maximum depth of approximately one hundred meters. For these reasons, there is a need to revise current hydrogeological models, which are based on tectonic fractures represented by lineaments.

As a result, particular attention has been paid to the fissured layer because it ensures the transmissive function of hard rock aquifers and is captured in most boreholes (Courtois *et al*., 2009). In this case study, the mean thickness is estimated at 13.8 ± 8 m using the lithologs. With ERT, its maximum estimated thickness is about 20 m. These values are globally lower than those obtained by Courtois *et al*. (2009) from hydrogeological data which are between 27 and 31 m on the same geological formations in Burkina Faso. Two main reasons may explain the underestimation of the fissured layer thickness: (i) the absence of precise lithologs for the boreholes. An uncertainty exists concerning the actual depth of the base of the saprolite; and (ii) the difficulty in choosing an electrical resistivity threshold to delineate the base of the fissured layer. This can be explained by the theory of percolation (e.g. Guéguen and Palciauskas, 1992). Indeed, the decrease in the density of fissures at the bottom results in stopping the percolation. It then becomes difficult to distinguish the electrical resistivities from the base of the fissured layer and those of the fresh rock.

The model developed in the present study is compared with the models proposed by Koïta *et al.* (2013), in Ivory Coast and Dewandel *et al.* (2006) in India. The geological formations studied in Ivory Coast and those of Sanon underwent the same geological history during the Eburnean orogenic cycle dated from 2400 to 1600 Ma (Lompo, 2010; Thiéblemont *et al.*, 2004). This comparison reveals similarities and differences, in terms of the geometry and structure of the profiles. Indeed, the weathering profile proposed in the present study is characterized, from top to bottom, by a vertical structure with three distinct layers, as proposed by Koïta et *al.* (2013): a saprolite layer, a fissured layer and the fresh rock. In both of these models, the layers are not stratiform at the scale of the catchment, suggesting that they were formed at different times (Dewandel *et al.*, 2006) or that they are influenced by differential weathering as green rocks were observed below the ridges of the study area. The layers have varying thicknesses whose spatial variations are enhanced by the recent topography of the sites. Indeed, the weathering profile of the Sanon site is characterized by a low thickness of saprolite at the ridges and much greater in the valley. This configuration is contrary to that observed in Ivory Coast (Koïta *et al.*, 2013; Avenard *et al.*, 1971), where the weathering profile is more complete and thicker on the ridges covered by an iron crust, and thinner in the valleys marked by a deepening of the river bed, which sometimes reveals fresh bedrock. In Ivory Coast, the weathering profile was surely (quite recently) eroded by the streams that now reach the fissured layer or the fresh rock where the stream incisions are quite deep. This is not the case in Burkina Faso in general (Courtois *et al.*, 2009), and at the Sanon site in particular where the topographic differences seem to be much less important as a consequence surely of a low erosion rate. The development of such profiles requires long periods of time during which the regions are characterized by a moderate relief (Lachassagne and Wyns, 2005).

Moreover, the iron crust covering the ridges show different landforms, whether in Sudano-Sahelian climatic conditions or in wet areas. In Sudano-Sahelian climatic conditions such as Sanon site, iron crust is in extensive and compact blocks which resisted the dismantling (Avenard *et al.*, 1971). However, in wet areas such as Ivory Coast, iron crust is often dislocated (existence of some residual blocks) or even completely dismantled following a lowering of the base level and a period of wetter climate (Avenard et al., 1971). Thus, in Sanon site, the iron crust covering the ridges promotes the surface flows giving rise to flows which can at times be torrential (Maignien, 1958). Thus, the valley becomes a preferential zone for infiltration and consequently for recharge. Infiltration in a valley would also be facilitated by a gentle slope, when this is insufficient to promote erosion of the valley, and would favor deep weathering by allowing water to persist for longer periods of time (Brideau *et al.*, 2009).

From the hydrogeological point of view, the consequence of this difference in the behavior of ridge to ridge weathering profiles is that the topographical and hydrogeological watersheds of the Sanon site are not superposed. In other words, the ridges do not coincide with the groundwater divides.

6. Conclusion

The weathering profile of the Sanon experimental site, whose geology is representative of West African hard rocks, has been characterized in terms of its geometry and structure. This reveals that the weathering profile (of granite and migmatite) is standard, with three main layers: a saprolite layer (composed of iron crust, alloterite and isalterite sub-layers), a fissured layer and a fresh rock.

In addition, this weathering profile is found to be similar to that of models proposed in recent years, which concluded that the hydraulic conductivity of hard rock aquifers is due to weathering processes, and not to tectonic fractures.

The profile from this study was compared with other profiles observed under a present humid tropical climate, with the same formations and the same geological history during the Eburnean orogenic cycle but different reliefs at the catchment scale. Various discrepancies are found in terms of their geometry and structure. At the Sanon site, the saprolite thickness is thus greater in the valley than at the level of the ridge, which is contradictory to the conditions observed under a present humid tropical climate, where the thickness of the saprolite is greater at the ridges.

Moreover, the lineaments observed in previous studies do not appear to be tectonic fractures, and are not clearly visible on the proposed 2D geological sections. The lack of correlation between the presence and location of tectonic lineaments and fractures could explain the high rate of negative boreholes in hard rock aquifers occurring in contexts where, during drilling campaigns, a well's location is systematically based on the study of local lineaments.

Acknowledgments

This research was carried out in the framework of the GRIBA project (Groundwater Resources In Basement rocks of Africa), funded by the African Union, the European Union, and the Institut de Recherche pour le Développement (IRD) (grant AURG/098/2012).

We wish to thank the IRD for financing a student study visit under the auspices of the BEST program, at the UMR Metis of the Pierre and Marie Curie - Paris 6 University in France.

We would also like to thank C. ALLE, Y. KONE, and S. MAIGA for their active involvement in our field study campaigns.

Mr P. LACHASSAGNE is thanked for his useful remarks and comments that improved the quality of the paper.

References

Avenard JM, Eldin M, Girard G, Sircoulon J, Touchebeuf P, Guillaumet JL, Adjanohoun E. 1971. Le milieu naturel de Côte d'Ivoire. Mémoire 50, ORSTOM, France.

BRGM-Aquater. 1991. Exploitation des eaux souterraines en socle cristallin et valorisation agricole : pilote expérimental en milieu rural pour les zones soudano-sahéliennes et sahéliennes. Rapport 33576. BRGM, France.

Brideau MA, Yan M, Stead D. 2009. The role of tectonic damage and brittle rock fracture in the development of large rock slope failures. *Geomorphology* **103** (1): 30–49 DOI: 10.1016/j.geomorph.2008.04.010

Brunner P, Franssen HJH, Kgotlhang L, Bauer-Gottwein P, Kinzelbach W. 2006. How can remote sensing contribute in groundwater modeling? *Hydrogeology Journal* **15** (1): 5–18 DOI: 10.1007/s10040-006-0127-z

Carter RC, Parker A. 2009. Climate change, population trends and groundwater in Africa. *Hydrological Sciences Journal* **54** (4): 676–689 DOI: 10.1623/hysj.54.4.676

Chapellier D. 1987. *Diagraphies appliquées à l'hydrologie*. Lavoisier: Paris.

Chaudhuri A, Sekhar M, Descloitres M, Godderis Y, Ruiz L, Braun JJ. 2013. Constraining complex aquifer geometry with geophysics (2D ERT and MRS measurements) for stochastic modelling of groundwater flow. *Journal of Applied Geophysics* **98**: 288–297 DOI: 10.1016/j.jappgeo.2013.09.005

Chilton PJ, Foster SSD. 1995. Hydrogeological characterisation and water-supply potential of basement aquifers in tropical Africa. *Hydrogeology Journal* **3** (1): 36–49

Compaoré G. 1997. Evaluation de la fonction capacitive des altérites: Site expérimental de Sanon (Burkina Faso) socle granito-gneissique sous climat de type soudano-sahélien. Thèse de doctorat, Université d'Avignon et des Pays Vaucluse, France.

Compaoré G, Lachassagne P, Pointet T, Travi Y. 1997. Evaluation du stock d'eau des altérites: expérimentation sur le site granitique de Sanon (Burkina Faso). *IAHS Publications-Series of Proceedings and Reports-Intern Assoc Hydrological Sciences* **241**: 37–46

Courtois N, Lachassagne P, Wyns R, Blanchin R, Bougaïré FD, Somé S, Tapsoba A. 2009. Large-scale mapping of hard-rock aquifer properties applied to Burkina Faso. *Ground Water* **48** (2): 269–283 DOI: 10.1111/j.1745-6584.2009.00620.x

Dahlin T. 2001. The development of DC resistivity imaging techniques. *Computer and Geosciences* **27** (9): 1019–1029 DOI: 10.1016/S0098-3004(00)00160-6

Dahlin T, Zhou B. 2004. A numerical comparison of 2D resistivity imaging with 10 electrode arrays. *Geophysical Prospecting* **52** (5): 379–398 DOI: 10.1111/j.1365-2478.2004.00423.x

Descloitres M, Ribolzi O, Troquer YL, Thiébaux JP. 2008a. Study of water tension differences in heterogeneous sandy soils using surface ERT. *Journal of Applied Geophysics* **64** (3–4): 83–98 DOI: 10.1016/j.jappgeo.2007.12.007

Descloitres M, Ruiz L, Sekhar M, Legchenko A, Braun JJ, Mohan Kumar MS, Subramanian S. 2008b. Characterization of seasonal local recharge using electrical resistivity tomography and magnetic resonance sounding. *Hydrological Processes* **22** (3): 384–394 DOI: 10.1002/hyp.6608

Dewandel B, Gandolfi JM, de Condappa D, Ahmed S. 2008. An efficient methodology for estimating irrigation return flow coefficients of irrigated crops at watershed and seasonal scale. *Hydrological Processes* **22** (11): 1700–1712 DOI: 10.1002/hyp.6738

Dewandel B, Lachassagne P, Wyns R, Maréchal JC, Krishnamurthy NS. 2006. A generalized 3D geological and hydrogeological conceptual model of granite aquifers controlled by single or multiphase weathering. *Journal of Hydrology* **330** (1–2): 260–284 DOI: 10.1016/j.jhydrol.2006.03.026

Dewandel B, Perrin J, Ahmed S, Aulong S, Hrkal Z, Lachassagne P, Samad M, Massuel S. 2010. Development of a tool for managing groundwater resources in semi-arid hard rock regions: application to a rural watershed in South India. *Hydrological Processes* **24** (19): 2784–2797

Egal E, Thiéblemont D, Lahondère D, Guerrot C, Costea CA, Iliescu D, Delor C, Goujou JC, Lafon JM, Tegyey M, Diaby S, Kolié P. 2002. Late Eburnean granitization and tectonics along the western and northwestern margin of the Archean Kénéma–Man domain (Guinea, West African Craton). *Precambrian Research* **117** (1–2): 57–84 DOI: 10.1016/S0301-9268(02)00060-8

Faillat JP, Blavoux B. 1989. Caractères hydrochimiques des nappes des roches endogènes fissurées en zone tropicale humide: l’exemple de la Côte d’Ivoire. *Journal of African Earth Sciences (and the Middle East)* **9** (1): 31–40 DOI: 10.1016/0899-5362(89)90005-5

Feybesse JL, Billa M, Guerrot C, Duguey E, Lescuyer JL, Milesi JP, Bouchot V. 2006. The paleoproterozoic ghanaian province: Geodynamic model and ore controls, including regional stress modeling. *Precambrian Research* **149** (3–4): 149–196 DOI: 10.1016/j.precamres.2006.06.003

Guéguen Y. and Palciauskas V. 1992. *Introduction à la physique des roches*. Hermann: Paris.

Guiraud R. 1988. L'hydrogéologie de l'Afrique. *Journal of African Earth Sciences (and the Middle East)* **7** (3): 519–543 DOI: 10.1016/0899-5362(88)90043-7

Günther T. 2004. Inversion methods and resolution analysis for the 2D/3D reconstruction of resistivity structures from DC measurements. PhD Thesis, University of Mining and Technology of Freiberg, Germany.

Kabré WP. 2012. Caractérisation hydrogéologique en milieu de socle fracturé : Cas de la province de Kourwéogo. Mémoire de master. Institut International d'Ingénierie de l'Eau et de l'Environnement de Ouagadougou, Burkina Faso.

Kamagaté B, Séguis L, Goné Droh L, Favreau G, Koffi K. 2008. Processus hydrogéochimiques et séparation d'hydrogrammes de crue sur un bassin versant en milieu soudano-tropical de socle au Bénin (Donga, haute vallée de l'Ouémé). *Journal of Water Science* **21** (3): 363–372

Koïta M, Jourde H, Koffi KJP, Silveira KSD, Biaou A. 2013. Characterization of weathering profile in granites and volcanosedimentary rocks in West Africa under humid tropical climate conditions. Case of the Dimbokro Catchment (Ivory Coast). *Journal of Earth System Science* **122** (3): 841–854 DOI: 10.1007/s12040-013-0290-2

Kouamé KF, Lasm T, De Dreuzy JR, Akaffou AG, Bour O, Davy P. 2010. Contribution d'un modèle hydrogéologique à fractures discrètes à l'étude des aquifères fracturés du socle Archéen de Touba (Nord-Ouest, Côte d'Ivoire). *Journal of Water Science* **23** (1): 41–56

Kouamelan AN, Djro SC, Allialy ME, Paquette JL, Peucat JJ. 2015. The oldest rock of Ivory Coast. *Journal of African Earth Sciences* **103**: 65–70 DOI: 10.1016/j.jafrearsci.2014.12.004

Lachassagne P, Wyns R. 2005. Aquifères de socle: nouveaux concepts - Application à la prospection et la gestion de la ressource en eau. *Géosciences* **2**: 32 – 37

Lachassagne P, Wyns R, Dewandel B. 2011. The fracture permeability of Hard Rock Aquifers is due neither to tectonics, nor to unloading, but to weathering processes. *Terra Nova* **23** (3): 145–161 DOI: 10.1111/j.1365-3121.2011.00998.x

Langman JB, Blowes DW, Sinclair SA, Krentz A, Amos RT, Smith LJD, Pham HN, Sego DC, Smith L. 2015. Early evolution of weathering and sulfide depletion of a low-sulfur, granitic, waste rock in an Arctic climate: A laboratory and field site comparison. *Journal of Geochemical Exploration* **156**: 61–71 DOI: 10.1016/j.gexplo.2015.05.004

Lompo M. 2010. Paleoproterozoic structural evolution of the Man-Leo Shield (West Africa). Key structures for vertical to transcurrent tectonics. *Journal of African Earth Sciences* **58** (1): 19–36 DOI: 10.1016/j.jafrearsci.2010.01.005

Lutz A, Thomas JM, Pohll G, McKay WA. 2007. Groundwater resource sustainability in the Nabogo Basin of Ghana. *Journal of African Earth Sciences* **49** (3): 61–70 DOI: 10.1016/j.jafrearsci.2007.06.004

MacDonald AM, Davies J. 2000. A brief review of groundwater for rural water supply in sub-Saharan Africa. Technical Report WC/00/33. British Geological Survey, United Kingdom.

Maignien R. 1958. Le cuirassement des sols en Guinée : Afrique occidentale. ORSTOM, France. Available at: http://www.documentation.ird.fr/hor/fdi:10817

Maréchal JC, Dewandel B, Subrahmanyam K. 2004. Use of hydraulic tests at different scales to characterize fracture network properties in the weathered-fractured layer of a hard rock aquifer. *Water Resources Research* **40** (11): W11508 DOI: 10.1029/2004WR003137

Massuel S, Favreau G, Descloitres M, Le Troquer Y, Albouy Y, Cappelaere B. 2006. Deep infiltration through a sandy alluvial fan in semiarid Niger inferred from electrical conductivity survey, vadose zone chemistry and hydrological modelling. *CATENA* **67** (2): 105–118 DOI: 10.1016/j.catena.2006.02.009

Olayinka AI, Yaramanci U. 2000. Assessment of the reliability of 2D inversion of apparent resistivity data. *Geophysical Prospecting* **48** (2): 293–316 DOI: 10.1046/j.1365-2478.2000.00173.x

Razack M, Lasm T. 2006. Geostatistical estimation of the transmissivity in a highly fractured metamorphic and crystalline aquifer (Man-Danane Region, Western Ivory Coast). *Journal of Hydrology* **325** (1–4): 164–178 DOI: 10.1016/j.jhydrol.2005.10.014

Sander P. 2006. Lineaments in groundwater exploration: a review of applications and limitations. *Hydrogeology Journal* **15** (1): 71–74 DOI: 10.1007/s10040-006-0138-9

Sattran V, Wenmenga U. 2002. *Géologie du Burkina Faso*. Czech Geological Survey.

Savadogo NA, Nakolendousse S, Diallo S. 1997. Étude comparée de l'apport des méthodes électromagnetiques MaxMin et électriques dans l'implantation des forages à gros débits dans les régions de socle cristallin du Burkina Faso. *Journal of African Earth Sciences* **24** (1–2): 169–181 DOI: 10.1016/S0899-5362(97)00034-1

Su N, Yang SY, Wang XD, Bi L, Yang CF. 2015. Magnetic parameters indicate the intensity of chemical weathering developed on igneous rocks in China. *CATENA* **133**: 328–341 DOI: 10.1016/j.catena.2015.06.003

Taylor R, Howard K. 2000. A tectono-geomorphic model of the hydrogeology of deeply weathered crystalline rock: evidence from Uganda. *Hydrogeology Journal* **8** (3): 279–294

Taylor RG, Koussis AD, Tindimugaya C. 2009. Groundwater and climate in Africa—a review. *Hydrological Sciences Journal* **54** (4): 655–664 DOI: 10.1623/hysj.54.4.655

Thiéblemont D, Goujou JC, Egal E, Cocherie A, Delor C, Lafon JM, Fanning CM. 2004. Archean evolution of the Leo Rise and its Eburnean reworking. *Journal of African Earth Sciences* **39** (3–5): 97–104 DOI: 10.1016/j.jafrearsci.2004.07.059

Vouillamoz JM, Lawson FMA, Yalo N, Descloitres M. 2014. The use of magnetic resonance sounding for quantifying specific yield and transmissivity in hard rock aquifers: The example of Benin. *Journal of Applied Geophysics* **107**: 16–24 DOI: 10.1016/j.jappgeo.2014.05.012

Wright EP, Burgess WG. 1992. The hydrogeology of crystalline basement aquifers in Africa. *Geological Society Special Publication* **66**: 1–27

Wyns R, Baltassat JM, Lachassagne P, Legchenko A, Vairon J, Mathieu F. 2004. Application of proton magnetic resonance soundings to groundwater reserve mapping in weathered basement rocks (Brittany, France). *Bulletin de la Société Géologique de France* **175** (1): 21–34.

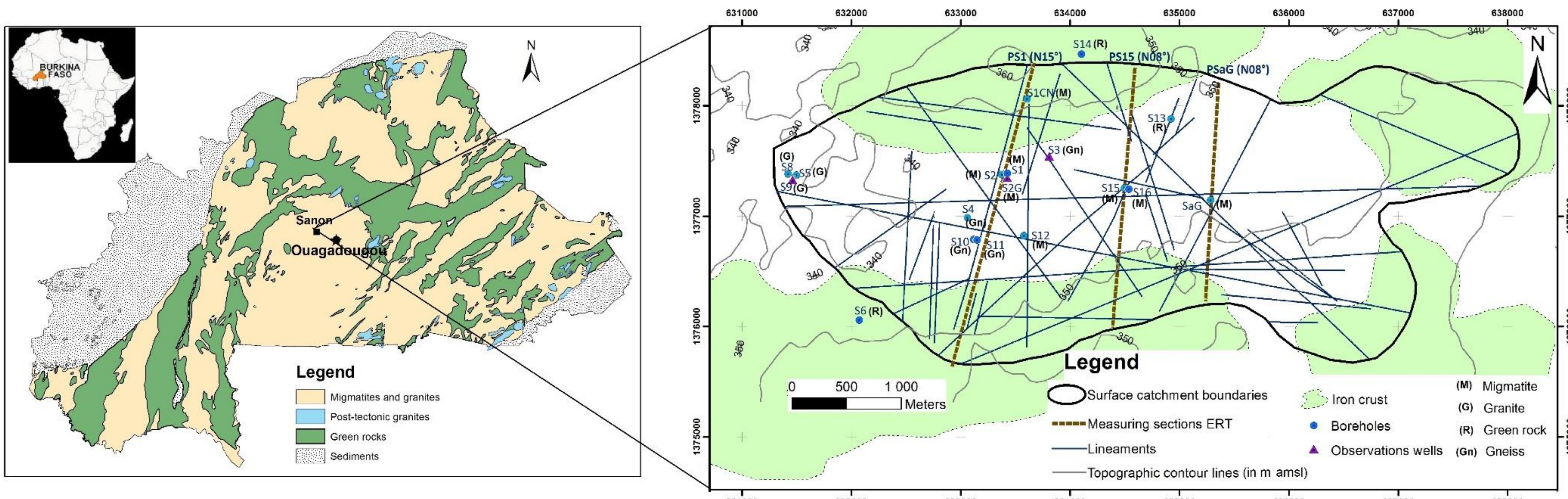

Figure 1: Location of the study site in Burkina Faso, Africa, showing the extent and locations of the iron crust, ERT sections, boreholes, observation wells, and lineaments within the surface catchment. Also, punctual location of geological formations using boreholes and observation wells.

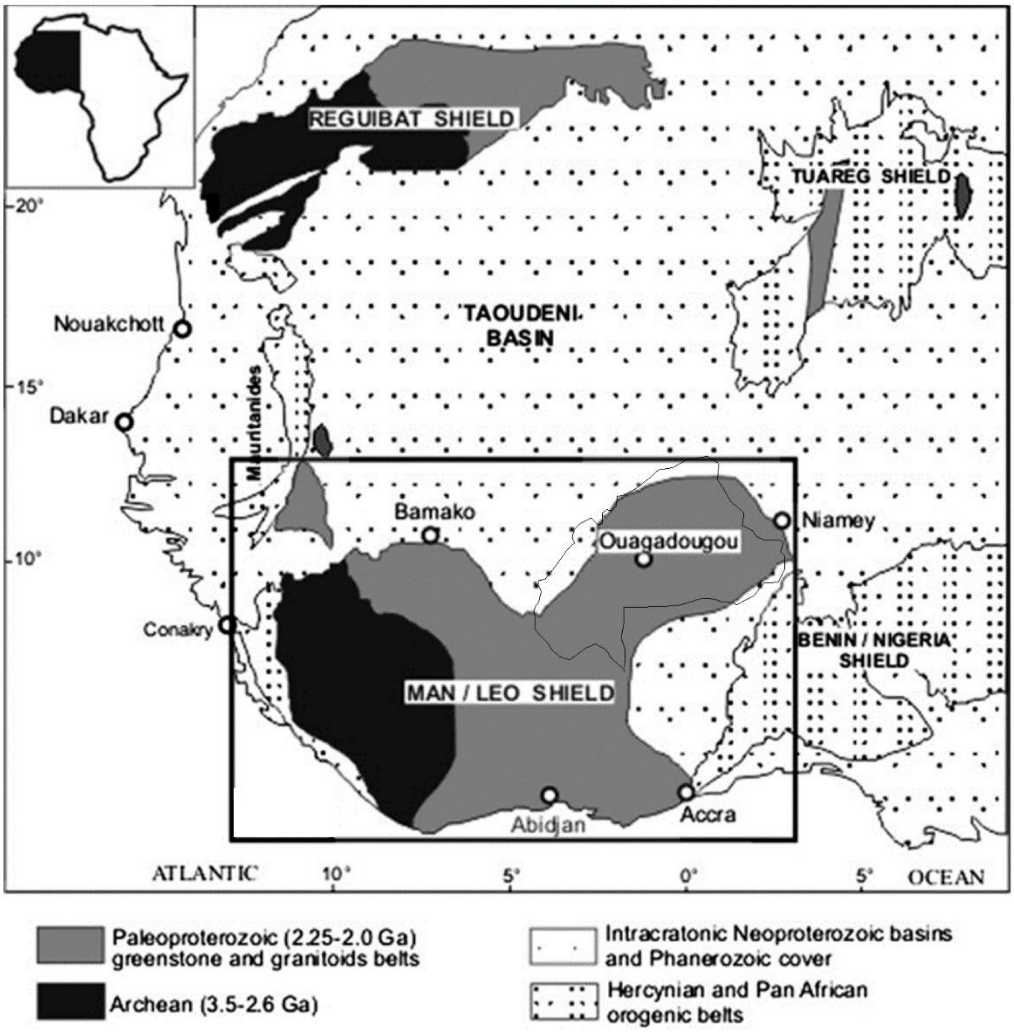

Figure 2: West African craton shown on a simplified geological map, and location of the Paleoproterozoic rocks (Lompo, 2010).

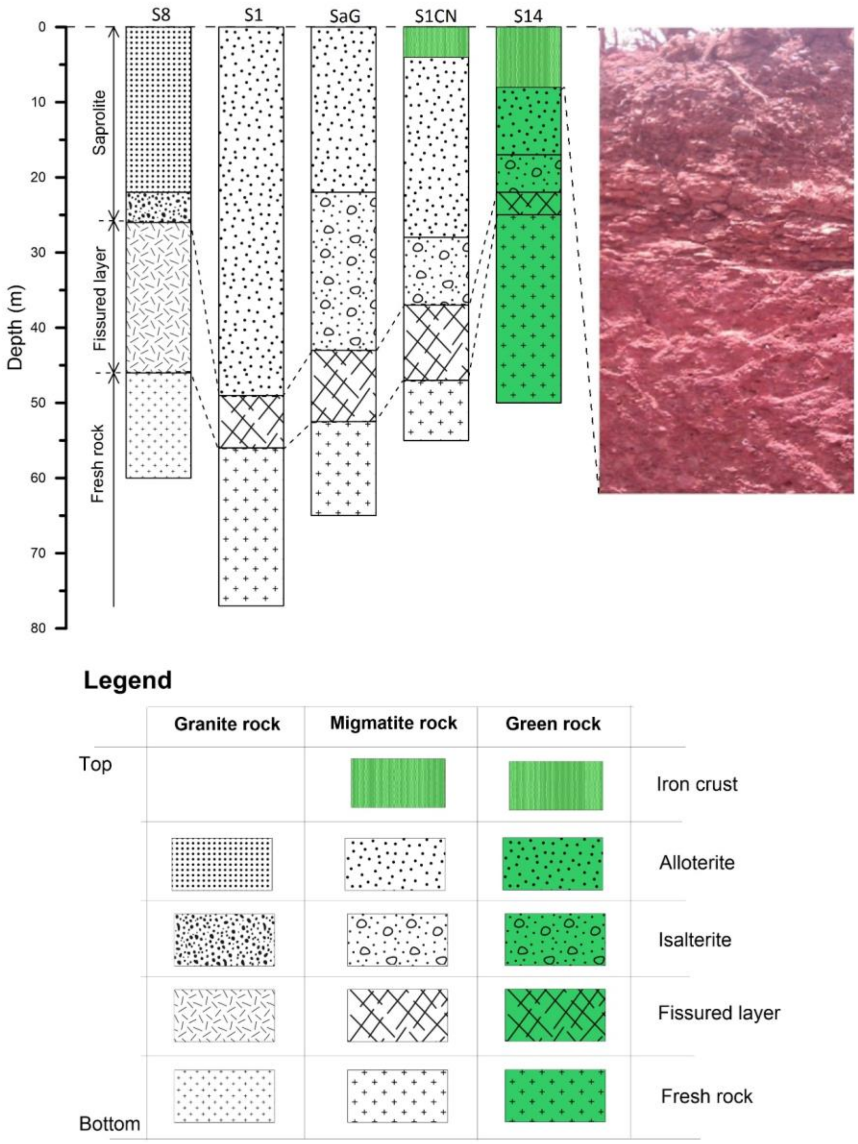

Figure 3: Examples of weathering profiles on granite, migmatite and green rock. The iron crust profile from a traditional brickwork is shown at the right of this figure. The height of the outcrop shown on the photograph is about 2 m.

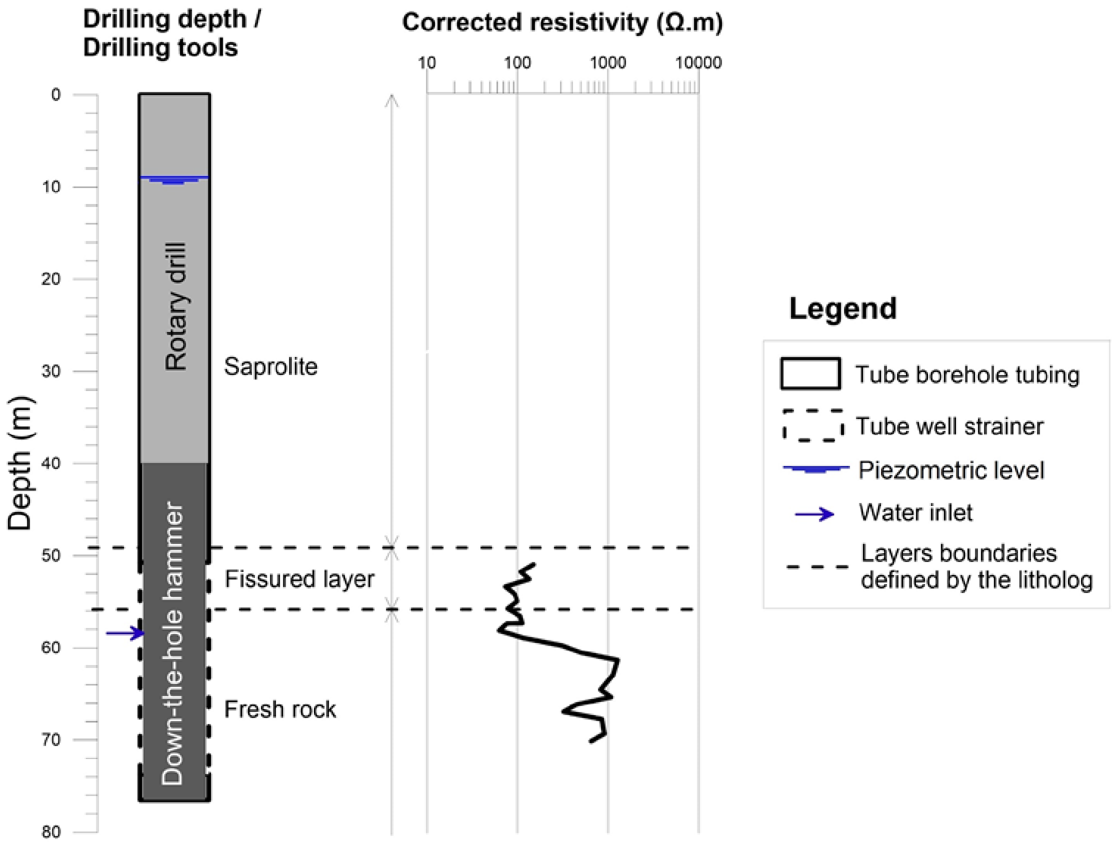

Figure 4: Variation of electrical resistivity as a function of depth in the S1 borehole. The measurements were only made along the part of the borehole with a perforated PVC casing.

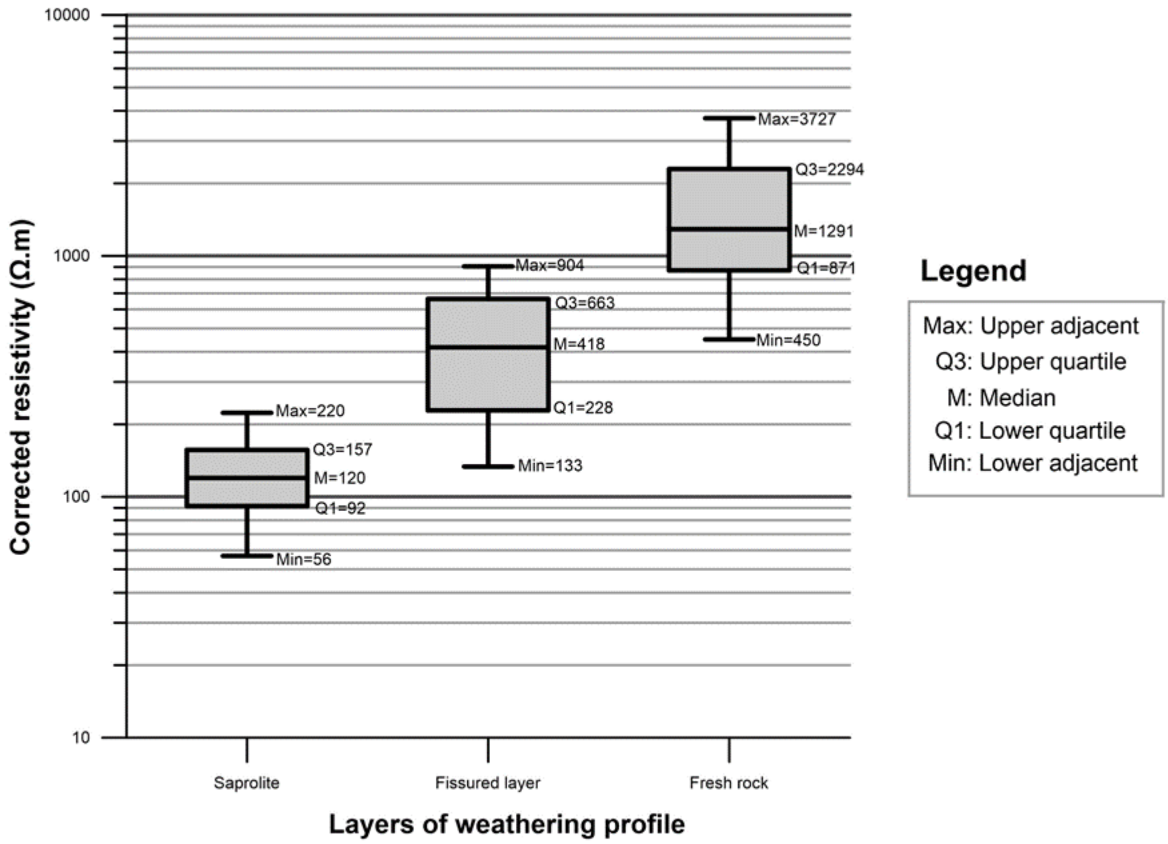

Figure 5: Corrected resistivity ranges, arranged according to the subsurface compartments of the weathering profile using the box plots.

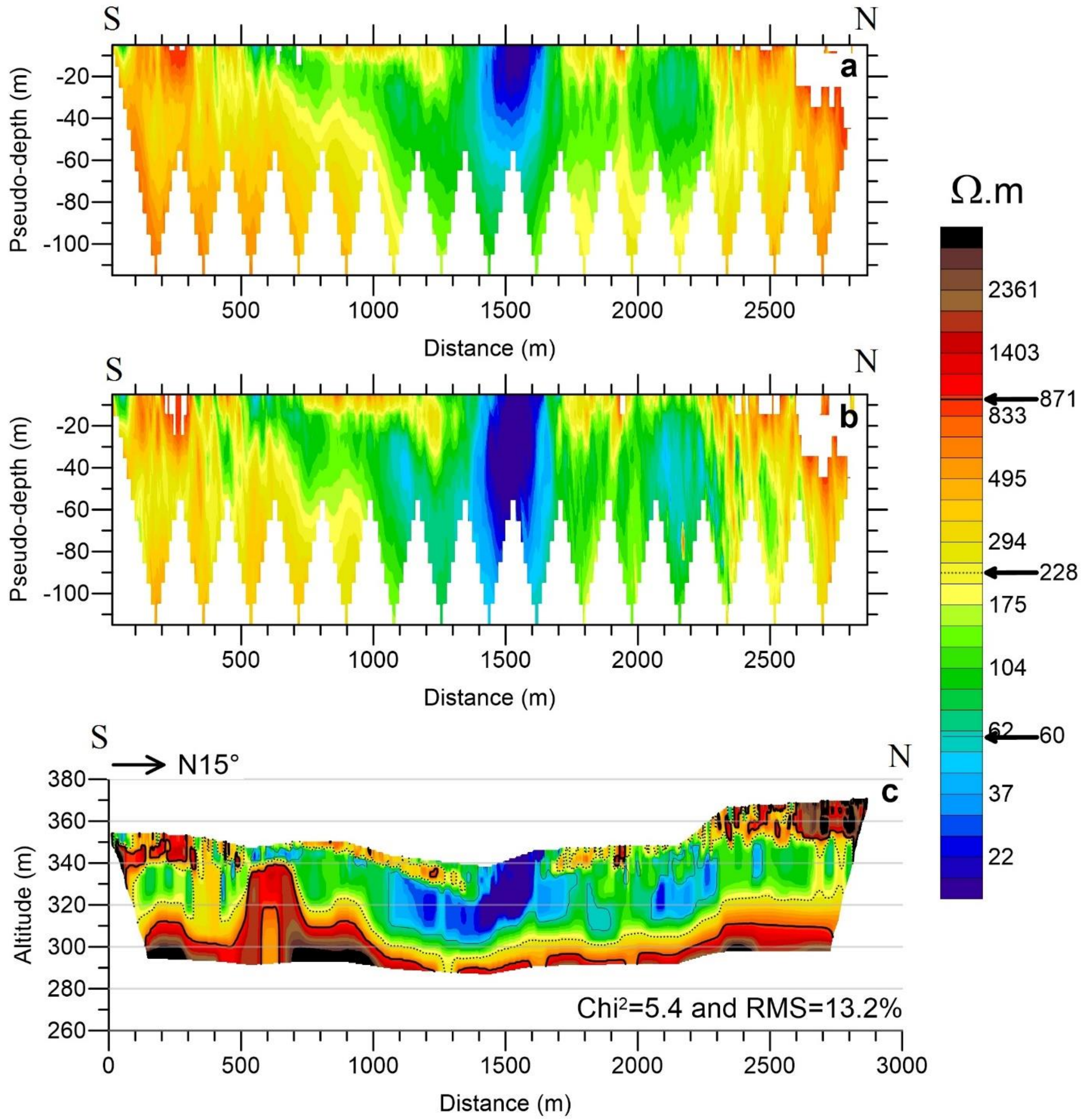

Figure 6: Example of PS1 profile: 2D apparent resistivity pseudo-sections measured with a) a Wenner-alpha array, and b) a Wenner-beta array. Figure 6c shows the interpreted 2D resistivity section, derived from the joint inversion of the two pseudo-sections.

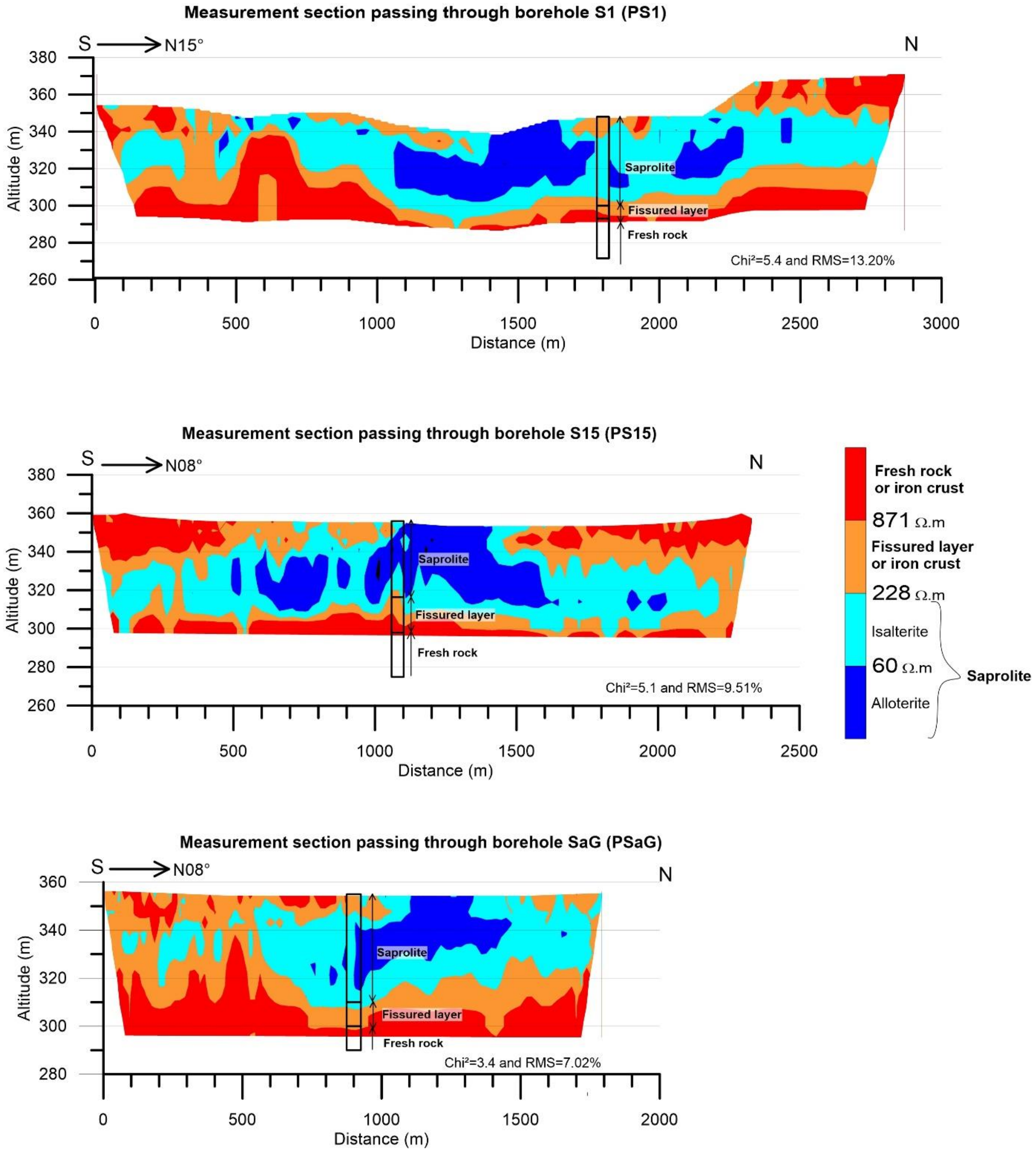

Figure 7: Classification of interpreted resistivities from the PS1, PS15 and PSaG profiles.

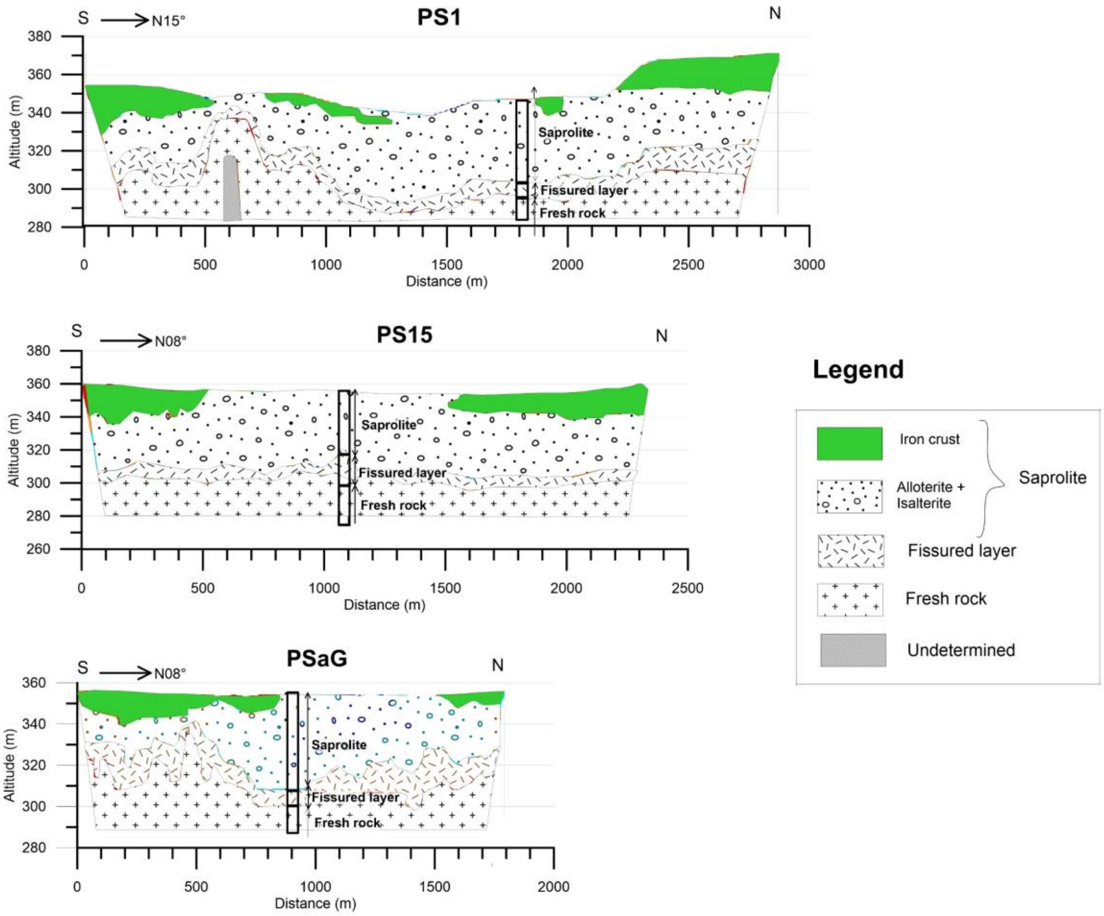

Figure 8: Geological models for the PS1, PS15 and PSaG profiles.